Mineralium Deposita (1997) 32: 581–595

ARTICLE

S. P. Kilias · J. Konnerup-Madsen

Fluid inclusion and stable isotope evidence for the genesis of quartz-scheelite veins, Metaggitsi area, central Chalkidiki Peninsula, N. Greece

Received: 8 April 1997 / Accepted: 8 July 1997

Abstract Scheelite mineralization accompanied by muscovite and albite, and traces of Mo-stolzite and stolzite occurs in epigenetic quartz vein systems hosted by two-mica gneissic schists, and locally amphibolites, of the Paleozoic or older Vertiskos Formation, in the Metaggitsi area, central Chalkidiki, N Greece. Three types of primary fluid inclusions coexist in quartz and scheelite: type 1, the most abundant, consists of mixed H_2O-CO_2 inclusions with highly variable (20–90 vol.%) CO_2 contents and salinities between 0.2 and 8.3 equivalent weight % NaCl. Densities range from 0.79 to 0.99 g/cc; type 1 inclusions contain also traces (< 2 mol%) of CH_4. Type 2 inclusions are nearly 100 vol.% liquid CO_2, with traces of CH_4, and densities between 0.75 and 0.88 g/cc. Type 3 inclusions, the least abundant, contain an aqueous liquid of low salinity (0.5 to 8.5 equivalent weight% NaCl) with 10–30 vol.% H_2O gas infrequently containing also small amounts of CO_2 (< 2 mol%); densities range from 0.72 to 0.99 g/cc. The wide range of coexisting fluid inclusion compositions is interpreted as a result of fluid immiscibility during entrapment. Immiscibility is documented by the partitioning of CH_4 and CO_2, into gas-rich (CO_2-rich) type 1 inclusions, and the conformity of end-member compositions trapped in type 1 inclusions to chemical equilibrium fractionation at the minimum measured homogenization temperatures, and calculated homogenization pressures. Minimum measured homogenization temperatures of aqueous and gas-rich type 1 inclusions of 220°–250 °C, either to the H_2O, or to the CO_2 phase, is considered the best estimate of temperature of formation of the veins, and temperature of scheelite deposition. Corresponding fluid pressures were between 1.2 and 2.6 kbar. Oxygen fugacities during mineralization varied from 10^{-35} to 10^{-31} bar and were slightly above the synthetic Ni-NiO buffer values. The fluid inclusion data combined with $\delta^{18}O$ water values of 3 to 6 per mil (SMOW) and $\delta^{13}C$ CO_2- fluid of −1.2 to +4.3 per mil (PDB), together with geologic data, indicate generation of mineralizing fluids primarily by late- to post-metamorphic devolatilization reactions.

Editorial handling: K. Shelton

S.P. Kilias (✉)
National University of Athens, Department of Geology,
Section of Economic Geology and Geochemistry,
Panepistimiopolis, Ano Ilissia, 15 784 Athens, Greece
e-mail:skilias@atlas.uoa.gr

J. Konnerup-Madsen
Geological Institute, University of Copenhagen,
Øster Voldgade 10, Copenhagen, DK-1350, Denmark

Introduction

Exploration for tungsten in the area of Metaggitsi, central Chalkidiki peninsula, North Greece (Fig. 1), has been carried out by BPMC (Bauxites Parnasse Mining Company, Greece) during 1963–1972, and between 1983 and 1988 by the Institute of Geology and Mineral Exploration (IGME) of Greece. Mineralization was discovered in 1965 by BPMC when soil geochemical prospecting, trenching and drilling delineated a mineralized zone approximately 1 × 3 km in extent containing some 10 major scheelite-bearing quartz veins and minor stratabound scheelite disseminations. Veranis and Bitzios (1984) in their study of the area, proposed that tungsten was most likely remobilized from pre-existing primary mineralization and introduced into the veins forming at the same time in the surrounding rocks.

This study presents mineralogical, fluid inclusion and oxygen and carbon isotope data in an attempt to decipher the nature and the origin of the mineralizing fluids, as well as the physicochemical conditions of formation of the quartz-scheelite vein mineralization in the area of Metaggitsi.

Regional geologic setting

Scheelite mineralization of the Metaggitsi area occurs mainly in the Vertiskos Formation that constitutes the western part of the Paleozoic or older Servo-Macedonian massif (Fig. 1) (Kockel et al.

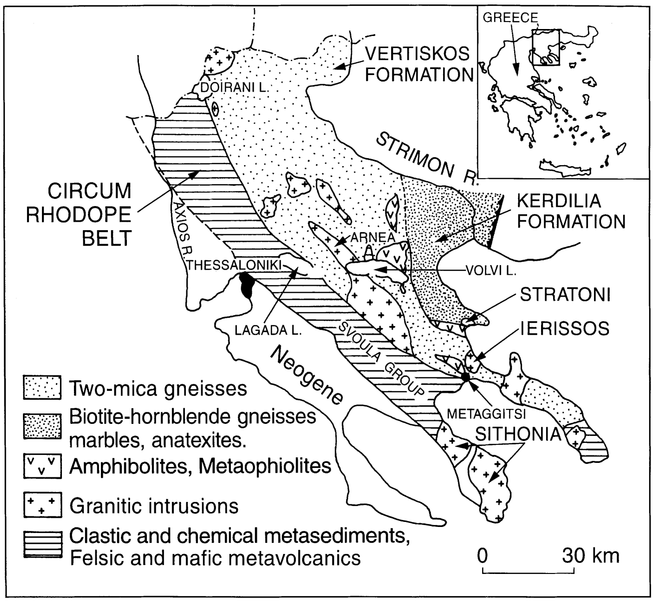

Fig. 1 Geotectonic map of the Servo-Macedonian Massif (modified after Kockel et al. 1977)

1977). East of the Vertiskos Formation is the tectonically underlying Kerdilia Formation (Fig. 1). Minor mineralization also occurs in rocks of the Svoula Group that outcrops within the southernmost extension of the young Paleozoic to early Mesozoic Circum Rhodope Belt (Kaufmann et al. 1976; Schuneman 1986), which constitutes a tectonic juxtaposition to the Servo-Macedonian massif in the west (Fig. 1).

The Vertiskos Formation is a NW-SE trending highly deformed and polymetamorphosed heterogeneous assemblage of conformable two-mica gneisses, augen gneisses, amphibolites, metaophiolitic rock complexes, and later granitic bodies (Kockel et al. 1977; Papadopoulos 1982; Dixon and Dimitriadis 1984; Sakellariou 1988). Studies of protoliths of the Vertiskos Formation indicate that the two-mica gneisses are of either volcano-sedimentary or sedimentary origin, and that the amphibolites are the metamorphic equivalents of basic tholeiitic rocks (Fournaraki 1981; Kougoulis 1986; Sakellariou 1988; Kougoulis et al. 1989). The Svoula Group consists of fossiliferous marbles of Upper Triassic age (Kaufmann et al. 1976) overlain by a metamorphosed flysch facies of Lower Jurassic age consisting of phyllitic and psammitic rocks, and quartzites (Kockel et al. 1977).

Regional metamorphic grade in the Vertiskos Formation reached a peak of amphibolite facies during Late Jurassic to Early Cretaceous times attaining pressures and temperatures of 5–8 kbar and 600–700 °C (Kockel et al. 1977; Papadopoulos 1982; Dixon and Dimitriadis 1984; Papadopoulos and Kilias 1985; Patras et al. 1986; Sakellariou 1988). Evidence for a higher metamorphic grade, probably Hercynian (?) eclogite facies, exists locally (Sakellariou 1988; Dimitriadis and Godelitsas 1991). The main tectonometamorphic event was followed by retrogression to the greenschist facies (upper and middle-lower) (Fournaraki 1981; Kougoulis 1986; Frei 1986; Sakellariou 1988) and Tertiary calc-alkaline magmatism. Conditions during the retrogressive greenschist facies were 4–5 kbar and 500–550 °C and 2–3 kbar and 350–450 °C for the upper and middle-lower conditions, respectively (Sakellariou 1988). The Svoula Group rocks have only been metamorphosed to the greenschist-amphibolite facies transition (Frei 1986).

The Tertiary calc-alkaline magmatism is exemplified by the Sithonia pluton (Rb-Sr model age of 50.4 ± 0.7 Ma by Christofides et al. (1990)), and the Ierissos pluton (uraninite age of 54.5 ± 0.3 Ma by Frei (1992)). The older (U-Pb-zircon age of 212 ± 7 Ma of Vital (1986)) Arnea granitic intrusion (Fig. 1) is thought to have been tectonically emplaced (Kockel et al. 1977).

Local geology

The geology of the Metaggitsi area has been described by Brauer (1984) and Veranis and Bitzios (1984) . The following account is based upon these sources in conjunction with personal field and microscope studies.

The Vertiskos Formation in the study area consists of: (1) E-W trending two-mica gneisses, and intercalated tourmaline, and/or garnet-bearing mica-schists, of possible pelitic protoliths; (2) amphibolites with compositions suggestive of basaltic precursors intercalated with biotite-epidote schists interpreted as basic metattufs, and (3) various muscovite-feldspathic schists of metavolcanic (metarhyolites, metarhyodacites) origin. Locally the tourmaline-bearing garnet-mica schists and the feldspathic schists are intercalated with cherts containing up to 0.5 m thick lenses of banded iron formation (BIF) (Fig. 2). Rare aplitic dikes were observed cutting the metamorphic lithologies in the area. The Svoula Group in the area consists of the following lithologies (Fig. 2): calcic schists, sericitic marble and phyllites of sedimentary origin, and epidote-actinolite-chlorite schists and feldspathic schists derived from felsic to intermediate volcanic precursors.

The rocks of both the Vertiskos Formation and Svoula Group in the region experienced two major (D_1 and D_2) and two minor secondary (D_3 and D_4) phases of deformation. D_1 generated the

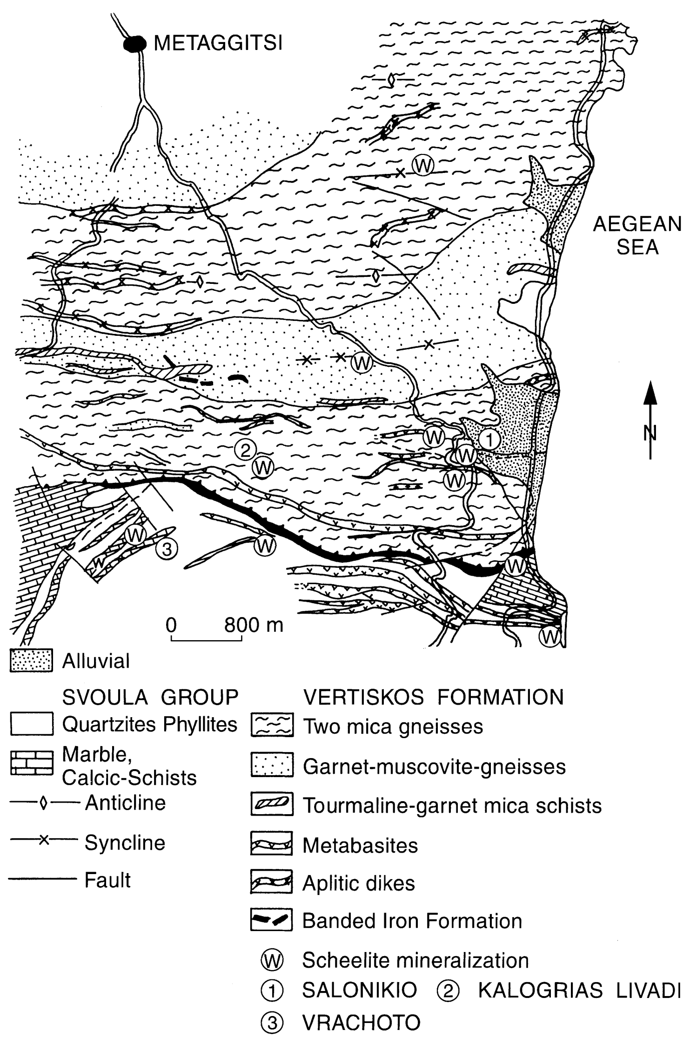

Fig. 2 Simplified geological map of the Metaggitsi area, central Chalkidiki Peninsula (Veranis and Bitzios 1984)

main, nearly E-W trending axial plane (S_1) schistosity in the region, whereas D_2 was a shearing deformation characterized by folding of the S_1 schistosity; it generated the major E-W trending regional anticlinal structure (Fig. 2). The last stages of the D_2 event or successive local scale D_3 and D_4 events are characterized by kink-banding deformation.

Mineralogical and textural data for the metabasites have revealed a retrograde, medium-grade amphibolite to low-grade greenschist facies metamorphism. The retrogressive greenchist facies was the last metamorphism to affect the lithologies in the area and is concomitant with the D_1 deformation. Comparative data suggest that this D_1 event is compatible with the last regional greenschist facies at pressures and temperatures of 2–3 kbar and 350–450 °C, respectively. D_2 was not associated with the formation of new minerals.

Tungsten mineralization

The rocks of the Metaggitsi area host two types of scheelite mineralization: a major vein-type, and a minor stratabound disseminated type.

Vein-type scheelite mineralization is contained within a complex swarm of quartz veins occupying fractures in the gneisses and schists, as well as in the amphibolites and basic metatuffs, in the Salonikio and Kalogrias-Livadi locations (Fig. 2). Veins at Salonikio trend NE-SW to E-W and crosscut, at low angles, the main schistosity of the hosting lithologies. At Kalogrias Livadi, crosscutting veins strike N-S to NE-SW. Veins measure up to 1 km in length (Kalogrias-Livadi) and are from a few centimetres to 1 m wide. Chemical assays from the veins at Salonikio indicate grades up to 0.5% WO_3 and less than 20 ppb Au.

Disseminated microcrystalline scheelite mineralization occurs parallel to schistosity of the basic metatuffs hosting the vein mineralization, at a small distance from the veins. Background concentration of W in the host metabasites, away from the mineralization and without microscopic scheelite, is about 100 ppm. Microscopic scheelite is concentrated within a narrow zone of 10 cm around the veins where the level of W increases to about 500 ppm. The host metabasites have high geochemical background of 100 ppm W which increases to about 500 ppm near the veins (N. Veranis, personal communication).

Wall-rock alteration around veins is moderate and is more visible in the gneiss than in other host rocks. It is characterized by thin (2–3 cm) quartz-muscovite ($\pm$ scheelite) selvages. Mineralogical changes have typically resulted in the destruction of plagioclase that is replaced by quartz and muscovite.

Scheelite also occurs in 0.2 to 5 cm wide quartz veinlets in the Svoula silicified marble in the Vrachoto area together with subordinate amounts of epidote and calcite.

Vein mineralogy

Quartz comprises about 95% of the veins. Scheelite occupies less than 1% by volume with other tungstates, muscovite, plagioclase, and minor sulfides and oxides being the principal accessories and locally accounting for up to 4%.

Tungstates

Scheelite in the gneiss-hosted veins is found as equant to elongate, anhedral to subhedral crystals up to 1 cm in length having straight to slightly curved borders with the host quartz (Fig. 3C, D).

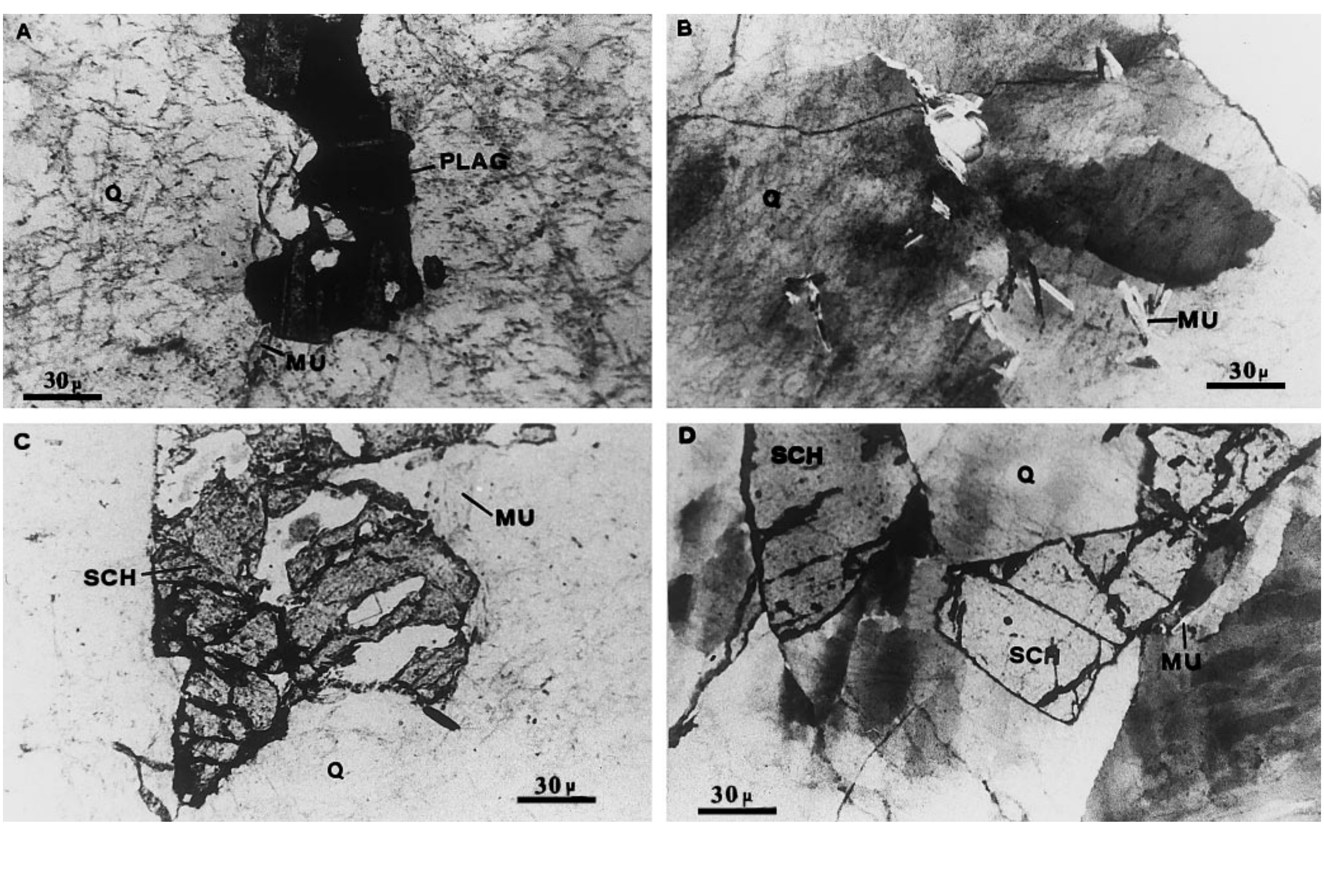

Fig. 3A–D Photomicrographs of vein paragenesis minerals and textures. **A** Undeformed twinned albite plagioclase (*PLAG*) in contact with muscovite (*MU*). **B** Randomly oriented crystals and monomineralic radiating crystal aggregates of muscovite (*MU*). **C** Polished section showing fractured scheelite (*SCH*) crystal in contact with muscovite (*MU*). Whitish patches are polishing effects due to removal of scheelite. **D** Fractured scheelite showing undulose extinction, **Q** vein quartz

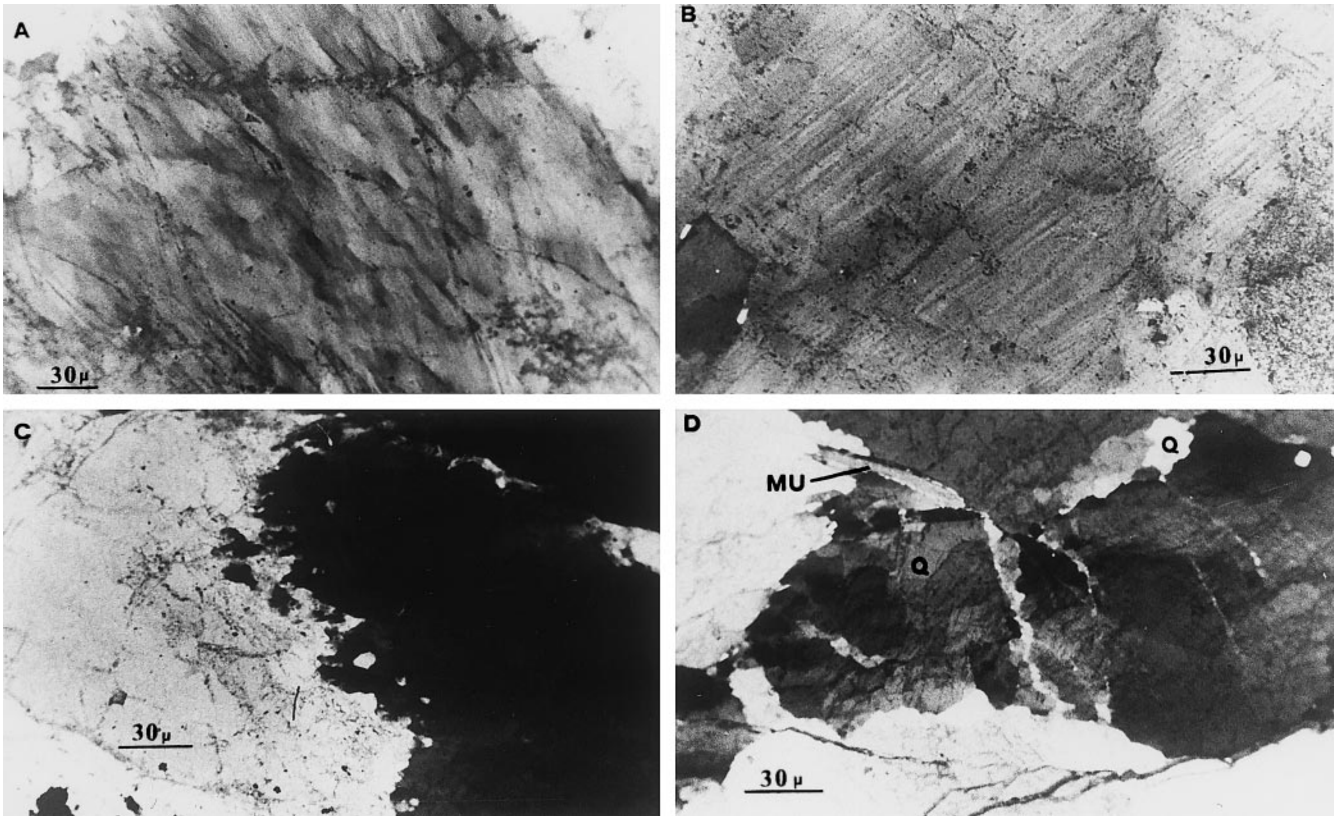

Scheelite crystals show undulose extinction and microfractures (Fig. 3C, D). The occurrence of scheelite in the marble-hosted veinlets is similar but the veinlets are also folded. Electron microprobe analyses (Kilias 1991) show that scheelite may contain less than 1 wt.% Mo. In addition subhedral grains of Mo-stolzite ($Pb_{0.99}(Mo_{0.39}W_{0.60})O_4$) were found. Both scheelite and Mo-stolzite have been replaced along fractures by stolzite ($(Pb_{0.96}Ca_{0.04})WO_4$. Minor arsenopyrite, pyrite and iron oxides are also found in veins.

Gangue

Quartz occurs in at least two generations in the paragneiss-hosted veins: (1) type I quartz with slight to moderate undulose extinction (Fig. 4A) with local sutured boundaries (Fig. 4C) and rarely fine lamellae which may be attributed to translation gliding phenomena (Fig. 4B) (Deer et al. 1966); (2) local subgrains and fine-grained recrystallized aggregates of quartz around grains with undulose extinction indicating incipient recrystallization (Fig. 4D); evidence of this type is rare.

On the basis of crystal interrelationships and similar deformation textures there is reasonable confidence that deposition of scheelite is coeval with type I quartz. Undeformed, twinned laths of albite to oligoclase occur in the veins in association with muscovite and quartz (Fig. 3A). Undeformed muscovite laths occur in association with scheelite (Fig. 3C, D), in monomineralic radiating aggregates within quartz crystals (Fig. 3B), and as isolated laths (Fig. 4D) crosscutting quartz grain boundaries.

Fluid inclusion study

Materials and methods

General fluid inclusion compositions and phase proportions were deduced from microscopy and microthermometry of type I quartz

Fig. 4A–D Photomicrographs of deformation microtextures in vein quartz. **A** Undulose extinction. **B** Translation gliding expressed as fine lamellae. **C** Sutured boundary between anhedral quartz crystals. **D** Fine grained recrystallized quartz aggregates around larger crystals with undulose extinction

and scheelite grains in 40 doubly polished 150–300 μm thick chips from scheelite-bearing quartz samples from both the Salonikio and Kalogrias Livadi locations. In addition, the gaseous phases in a smaller number of the fluid inclusions were analyzed by Raman microprobe spectrometry. Finally, the $\delta^{13}C$ isotope composition of inclusion fluids was obtained on 12 of the scheelite-bearing samples.

Microthermometry

Microthermometry was performed with a Chaixmeca heating and freezing stage (Poty et al. 1976), calibrated using commercially available chemical standards, at the Petrological Institute, University of Copenhagen, Denmark. The accuracy of measurements was determined to be better than ±0.5 °C over the temperature range of −70 °C to +30 °C and ±5 °C for higher temperatures.

Raman microprobe spectrometry

Analysis of the non-aqueous part of a smaller number of fluid inclusions was performed with a Jobin-Yvon MOLE Raman microprobe (Delhaye and Dhamelincourt 1975) at the CREGU, Nancy, France, using the 514.5 nm green line from a 5 W Spectra-Physics ionized argon laser as exciting radiation. A Leitz PLX100 water immersion objective was used.

δ^{13} C isotope analysis

The $\delta^{13}C$ isotope values of CO_2 contained in fluid inclusions from twelve (12) scheelite-bearing quartz samples were measured on a

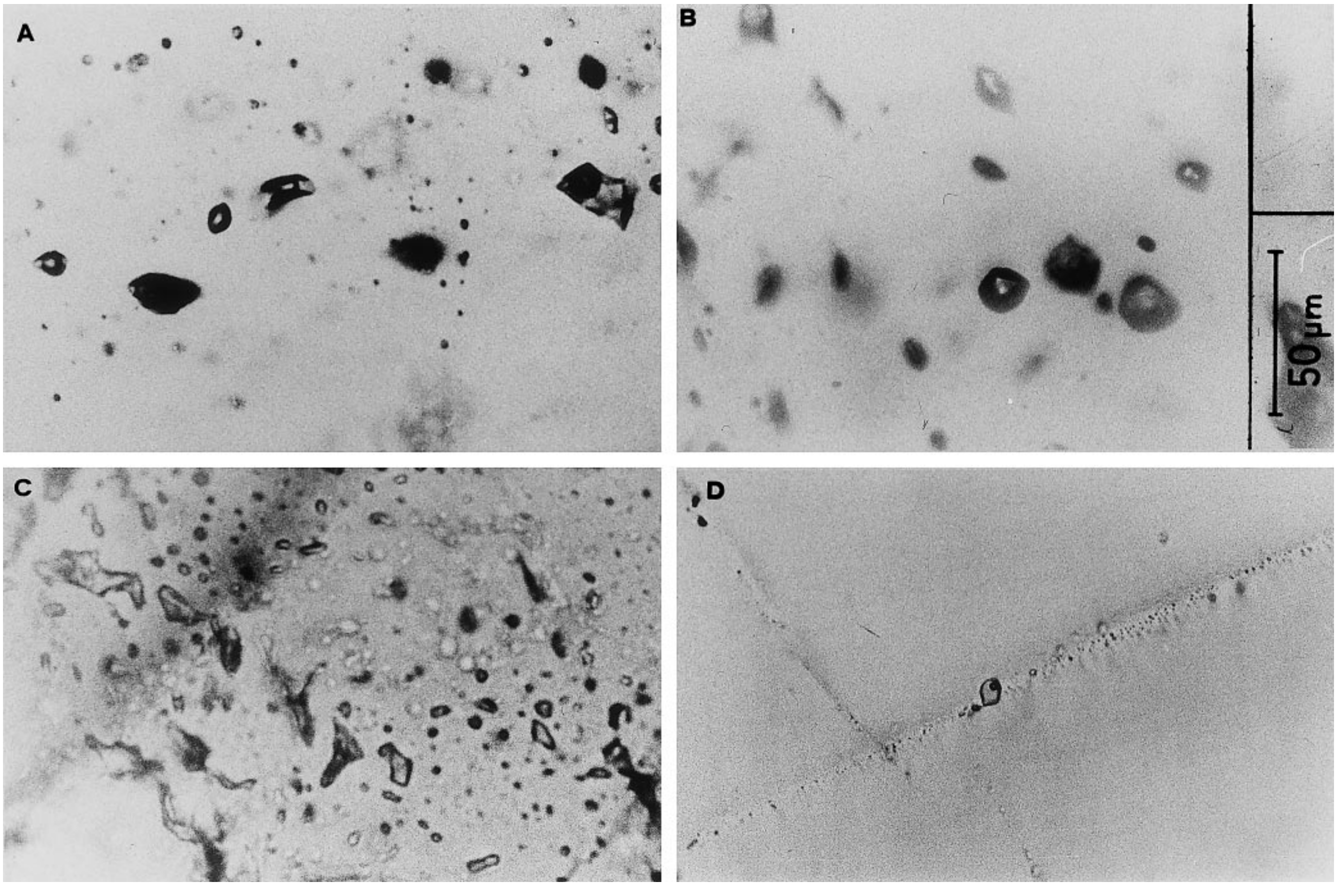

Fig. 5A–D Fluid inclusion characteristics. **A** Primary type 1 inclusions with highly variable CO_2/H_2O volume ratios coexisting with type 2 inclusions in quartz. **B** Primary type 1 inclusions in scheelite, obstracted observation is due to internal reflections. **C** Three-dimensional cluster largely composed of monophase liquid CO_2 type 2 inclusions in quartz. **D** Healed fracture containing secondary type 3 aqueous inclusions in quartz

Micromass 602C double collecting dual gas-feed mass spectrometer at the Department of Geochemistry, University of Utrecht, The Netherlands. Each sample selected for isotopic analysis was first examined petrographically to determine that it contained predominantly one type of fluid inclusion (see also Fig. 5A, C). Then fluid inclusions were opened by crushing 40–50 g sample under vacuum in copper tubes. The CO_2 was condensed in a liquid nitrogen cooled trap, and the non-condensable gases were removed. Subsequently, the CO_2 was separated at acetone melting temperature (−94.6 °C) and collected for mass spectrometry analysis. Semi-quantitative analyses of the fluid inclusion gases extracted for carbon isotope analyses using the scan facilities of the stable isotope mass spectrometer confirmed that the separated condensate was CO_2. Replicate analyses on different parts of eight quartz samples deviate from 0.0 to 0.5‰, suggesting acquisition of carbon isotope data with sufficient resolution.

Compositional types of fluid inclusions

Fluid inclusion data were obtained from the examination of 40 fluid inclusion wafers prepared from type I quartz and scheelite from both the Salonikio and Kalogrias Livadi locations. Three types of fluid inclusions have been identified both in type I quartz and scheelite: mixed type aqueous-carbonic inclusions (type 1), carbon dioxide inclusions (type 2), and aqueous inclusions (type 3):

Type 1 aqueous-carbonic fluid inclusions are characterized at room temperature by visible amounts of both undersaturated aqueous liquid plus carbon dioxide and consist either of three phases (liquid H_2O + liquid CO_2 + CO_2-rich vapour) or two phases (liquid H_2O + CO_2-rich liquid/vapour) (Fig. 5A). The vol.% of the CO_2 phase, as estimated visually at +30 °C, range from 20 to 90, but most inclusions contain between 30 and 50 vol.% CO_2. A few type 1 inclusions contain unidentified trapped non-metallic solids of various shapes and sizes.

Type 2 CO_2 fluid inclusions are present at room temperature either as one-phase liquid inclusions that nucleate a vapour bubble on cooling (Fig. 5C), or as two-phase (liquid + vapour) inclusions. Although not visually observed, some of the CO_2 inclusions contain a film of water lining the inclusion walls, as indicated by clathrate hydrate melting characteristics (see later).

Type 3 aqueous fluid inclusions at room temperature contain both a liquid and a vapour phase. The vapour bubble typically occupies 10–30 vol.% of the inclusion volume. Clathrate hydrate melting characteristics observed in a small number of type 3 inclusions (see later), however, indicate that some of the type 3 inclusions actually contain traces of CO_2 (up to 2.2 mol%) (Hedenquist and Henley 1985).

Type 1 inclusions are by far the most abundant followed by types 3 and 2 in decreasing frequency of occurrence. All inclusion types may have regular, elliptical, rounded or negative crystal shapes, or may be irregular. Most fluid inclusions are small with sizes ranging between 10 and 20 μm in their longest dimension.

Occurrence of fluid inclusions

Almost all the studied fluid inclusions are hosted by clear grains or crystal domains of type I quartz and intimately associated scheelite grains. Type II quartz is too fine-grained to contain workable inclusions.

Fluid inclusions in quartz may occur as: (a) irregular seemingly random clusters of inclusion types 1, 2, and 3, (b) single isolated type 1 inclusions, (c) irregular groups of type 1 inclusions with different volume % CO_2, (d) irregular clusters only containing types 1 or 2 inclusions (Fig. 5C). These types of fluid inclusion occurrences conform to those suggested for primary inclusions (Roedder 1984). Most type 3 inclusions occur as trails along narrow healed fractures (Fig. 5D) and are of secondary origin.

Fluid inclusions in scheelite appear mostly dark due to internal reflections (Fig. 5B) and occur either in random clusters (primary inclusions) or in short planar arrays within individual grains (pseudosecondary inclusions).

No systematic differences were observed in fluid inclusion characteristics in the different samples or between the Salonikio and the Kalogrias-Livadi locations.

Microthermometry results

Only primary or pseudosecondary inclusions were selected for microthermometry work, and most data were obtained on fluid inclusions in quartz I.

Type 1 aqueous-carbonic inclusions

Melting temperatures of solid CO_2 (Tm CO_2) in type 1 inclusions (Fig. 6A) range from −60.4 °C to −56.5 °C, suggesting the presence of gas other than CO_2 alone. The low-temperature behaviour of the carbonic phase indicated the additional component to be CH_4. This was confirmed by Raman Microprobe Spectrometry (see later). Homogenization temperatures of the CO_2 liquid and vapour phases (Th CO_2) show a considerable range from +4.5 to +26.7 °C, with a bimodal distribution (Fig. 6B). The CO_2 liquid and vapour phases homogenized to the liquid phase except for two inclusions that showed homogenization to the vapour phase at +18 °C and +26 °C (not included in Fig. 6B). Finally, four critical homogenizations were observed between +26.5 °C and 28 °C. This departure from the critical

Fig. 6A–D Low and high temperature microthermometry data on type 1 and 2 inclusions as indicated in the diagrams. **A** Temperatures of final melting of CO_2. **B** Temperatures of homogenization of CO_2 liquid and vapour; all homogenizations into the liquid phase. **C** Temperatures of final melting of clathrate in type 1 inclusions. **D** Temperatures of homogenization to liquid (*L*) or vapour (*V*), and temperatures of decrepitation of type 1 inclusions

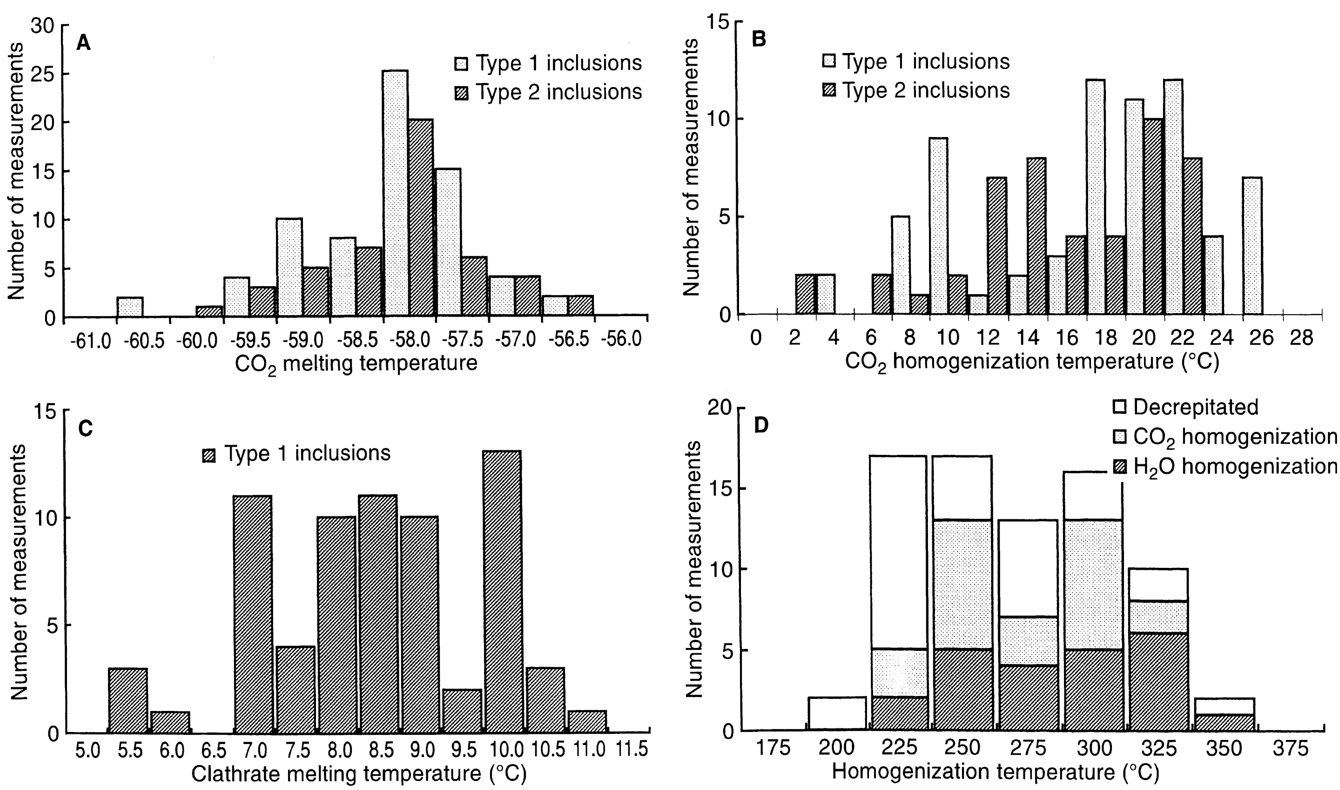

temperature of +31.2 °C for pure CO_2 can similarly be attributed to the presence of CH_4 (Burruss 1981).

Interpreted in terms of binary CO_2-CH_4 compositions, the combined melting and homogenization temperatures of the carbonic phase indicate contents of CH_4 ranging from 2 to 17 mol %, and the critical homogenization temperatures suggest contents between 3 and 5 mol % CH_4 (van den Kerkhof 1990). The homogenization temperatures and compositions of the carbonic fluids correspond to densities from 0.75 to 0.85 g/cc. These homogenization temperatures correspond to CO_2 densities ranging from 0.68 to 0.90 g/cc (median value 0.78 g/cc) (Fig. 6B) (Angus et al. 1976).

Initial and final melting temperatures of ice were very difficult to observe due to the small size of the inclusions and has not been recorded. Temperatures of melting of clathrate hydrate (Tm Clath) in the presence of both liquid and vapour CO_2 range from +5.5 °C to 11.1 °C (Fig. 6C). The deviations of univariant clathrate hydrate melting temperatures from that at +10.1 °C in the pure CO_2-H_2O system may be due to the presence of salts (e.g. NaCl) and CH_4. Interpreted in terms of ternary H_2O-NaCl-CO_2 compositions, the clathrate hydrate melting temperatures recorded below +10.1 °C correspond to salinities between 0.2 and 8.3 equivalent weight % NaCl (median value 3.9 equivalent weight % NaCl) (Collins 1979). The few clathrate melting temperatures higher than 10.1 °C are attributed to the presence of CH_4 in addition to CO_2 (Burruss 1981). In view of the indicated presence of CH_4 in most type 1 inclusions, the salinities of the aqueous phase given represent minimum values.

Total homogenization temperatures for type 1 inclusions vary between 220 °C and 345 °C and homogenization to both liquid and vapour was observed (Fig. 6D); homogenization to liquid occurred in the range 220 °C to 315 °C (median value 273 °C) and homogenization to vapour occurred between 220 °C to 345 °C (median value 293 °C). Homogenization temperatures in either phase cluster between 240 °C to 310 °C. A large number of the inclusions decrepitated before anticipated homogenization (estimated visually) at temperatures ranging from 188 °C to 336 °C (median value 250 °C) (Fig. 6D) demonstrating that decrepitation occurred at temperatures very close to total homogenization.

Due to the difficulties in observing phase changes in inclusions in scheelite because of internal reflections, microthermometry data from scheelite-hosted inclusions are limited. However, no systematic difference in microthermometry data was found between quartz and the limited workable scheelite-hosted inclusions and the data have therefore been treated collectively.

Type 2 carbonic fluid inclusions

CO_2 melting and homogenization temperatures for type 2 fluid inclusions are included in Fig. 6A, B, respectively. Melting temperatures range from −59.5 °C to −56.6 °C and indicate the presence of small amounts of CH_4 in some of the inclusions. A large spread in homogenization temperatures is observed (Fig. 6B) both within the individual sample and among samples. All homogenizations occurred in the liquid phase and correspond to densities from 0.78 to 0.88 g/cc (Angus et al. 1976).

Type 3 aqueous fluid inclusions

Temperatures of final melting of ice (Fig. 7A) in type 3 inclusions range from −5.5 °C to −0.3 °C (median value −3.0 °C) indicating salinities of 0 to 8.5 equivalent weight % NaCl (median value 5%) (Potter et al. 1978). Temperatures of first melting of ice at temperatures between −22 °C and −30 °C suggest the presence of dissolved KCl and/or $CaCl_2$/$MgCl_2$ in addition to NaCl (Crawford 1981). A few inclusions showed melting phenomena at temperatures above 0 °C and are interpreted in terms of low CO_2 contents in these type 3 inclusions (Hedenquist and Henley 1985); this was later confirmed by Raman analyses (see later). Temperatures of homogenization (always to the liquid phase) were between 110 °C and 233 °C (Fig. 7B); temperatures show two distinct peaks at 150 °C and 240 °C. The higher temperature peak corresponds to those type 3 inclusions coexisting with type 1 inclusions; some of these also exhibited clathrate melting phenomena. The lower temperature peak corresponds to apparently sec-

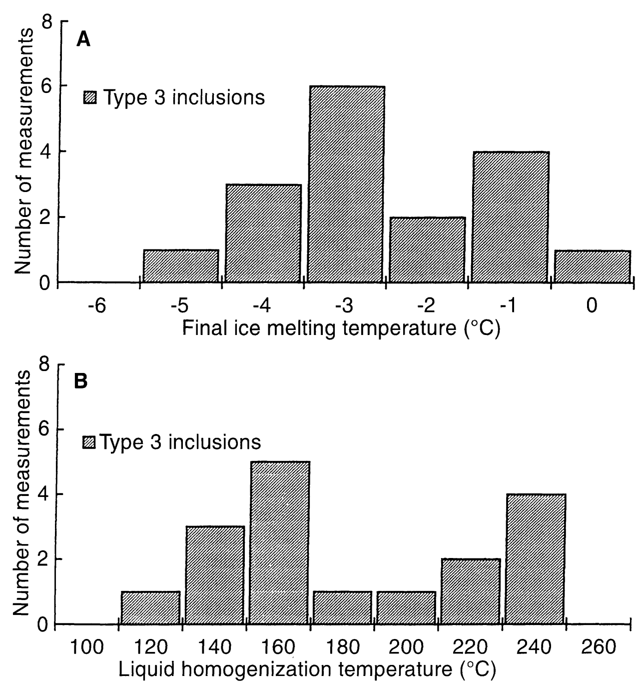

Fig. 7A, B Microthermometry data on type 3 inclusions in quartz **A** Temperatures of final ice melting in type 3 inclusions. **B** Temperatures of homogenization (to liquid) of type 3 inclusions ondary type 3 inclusions with irregular and serrated outlines exclusively occurring in healed fractures.

The aqueous type 3 inclusions have a density range of 0.80 to 0.99 g/cc (median value 0.93 g/cc) when calculated using the Ramboz et al. (1985) method. The possible presence of up to 2.2 mol% CO_2 in some of these inclusions would decrease the density by 0.03–0.05 g/cc.

Raman microprobe analysis

The composition of the carbonic, non-aqueous part of a small number of selected fluid inclusions previously examined by microthermometry was determined by Raman microprobe spectrometry. The results are presented in Table 1 together with the microthermometry data obtained on the same fluid inclusions. The measurements were always made at a temperature slightly higher than homogenization of the CO_2 phases. Although a search was made for a range of gaseous species, only two gases were identified by their Raman lines: CO_2 ($v = 1388\ cm^{-1}$) and CH_4 ($v = 2917\ cm^{-1}$) (Herzberg 1951). A high Raman signal ($30\ 000\ cm^{-1}$) in some inclusions suggested the presence of fluorescent hydrocarbons (naphthalene?).

In Table 1, the Raman analyses in terms of CO_2-CH_4 compositions are presented together with estimates of the CO_2-CH_4 compositions based on the microthermometry data. Inspection of Table 1 shows that the CH_4 contents estimated from microthermometry were always higher than those obtained from Raman spectrometry.

Compositions, bulk densities and molar volumes of type 1 inclusions

The molar fractions of H_2O, CO_2, CH_4 and NaCl, and the bulk densities and molar volumes of the examined fluid inclusions were calculated using the Ramboz et al. (1985) method and the Raman spectrometry and microthermometry data. The results are given in Table 2 for the eight inclusions presented in Table 1.

In Fig. 8, bulk inclusion densities and total homogenization temperatures of type 1 inclusions are presented. Calculated bulk densities range from 0.79 to 0.99 g/cc (median value 0.90 g/cc) (Fig. 8A). A negative correlation between the bulk density and bulk CO_2 molar composition in the H_2O-CO_2-NaCl system is indicated for type 1 inclusions (Fig. 8A); possibly two trends can be identified, one at higher and one at lower bulk densities for intermediate and high contents of mole% CO_2. The CH_4 content of the non-aqueous part (generally less than 2 mol% of bulk inclusion fluid) was ignored but this does not introduce any significant errors in the calculations (e.g. Konnerup-Madsen et al. 1985, Bottrell et al. 1988).

Table 1 Microthermometry data and the compositional and physical data calculated from the microthermometry data for eight(8) representative fluid inclusions in scheelite-bearing quartz

Inclusion number	Type	Volume % gas (CO_2/CH_4)	Microthermometry data (°C)			Aqueous fluid		Mol% CH_4 and molar volume of CO_2-CH_4 fluid		
			Tm,CO_2	Tm,Clath	$Th,CO_2(L)$	wt.% NaCl	Density, g/cc	Microthermometry	Raman	Molar volume, cm^3
1	1	90	−57.3	8.0	17.0	3.95	1.029	3.8	1.7	57.9
2	1	45	−60.0	−10.8	3.0	–	–	17.2	7.8	54.1
3	1	45	−57.3	8.3	19.0	3.00	1.017	3.7	0.7	56.4
4	1	10	−58.2	9.2	20.0	1.63	1.007	9.0	1.5	67.1
5	1	25	−57.8	8.0	17.0	3.95	1.022	4.0	0.8	62.5
6	1	90	−56.8	8.0	20.6	3.95	1.030	1.8	0.2	59.6
7	2	95	−57.5	8.5	9.0	2.30	1.020	5.1	0.6	54.7
8	3	25	–	–	–	0.40	–	–	–	–

Tm,CO_2: melting temperature of solid CO_2, Tm,Clath: melting temperature of clathrate hydrate, Th,CO_2: homogenization temperature of CO_2–CH_4 phase, L:homogenization in liquid phase

Table 2 Raman microprobe spectrometry results and calculated bulk fluid inclusion physical and chemical data for the same inclusions in quartz listed in Table 1

Inclusion		Raman spectroscopy		Bulk density and molar volume		Bulk chemical composition, mol%			
Number	Type	Mol% CO_2	Mol% CH_4	g/cc	cc/mole	H_2O	NaCl	CO_2	CH_4
1	1	98.3	1.7	0.78	47.5	25.5	0.4	72.5	1.5
2	1	92.2	7.8	0.95	25.5	73.2	–	24.9	1.9
3	1	99.2	0.8	0.91	25.9	76.4	0.7	22.5	0.2
4	1	98.5	1.5	0.99	19.3	92.8	0.9	6.2	0.03
5	1	99.2	0.8	0.94	22.7	87.1	1.4	11.3	0.09
6	1	99.7	0.3	0.80	43.1	34.5	0.7	64.6	0.1
7	2	99.3	0.7	0.89	39.9	32.5	0.2	69.9	0.5
8	3	96.3	3.7	0.77	24.4	96.6	–	3.3	–

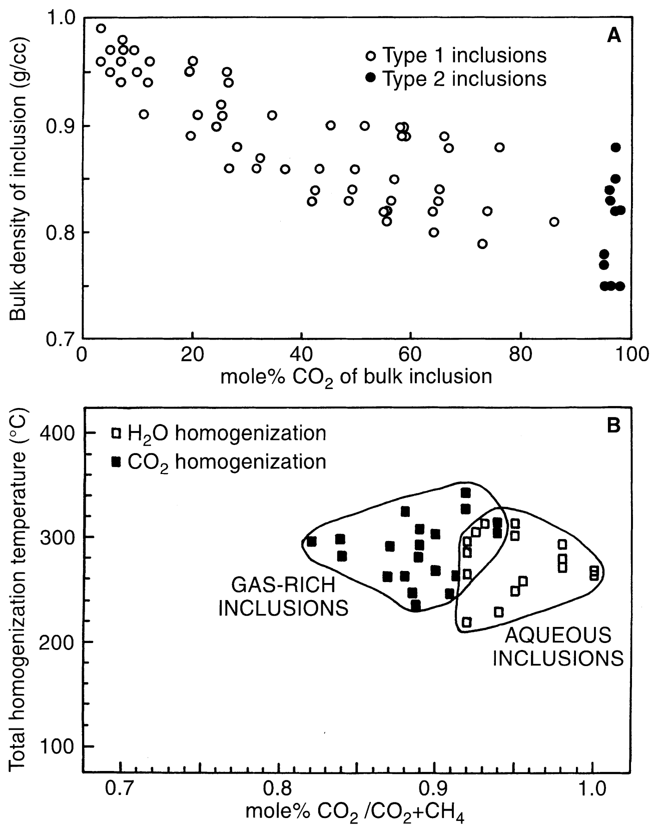

Fig. 8 **A** Bulk density (in g/cc) versus calculated mol% CO_2 content of type 1 and 2 inclusions. **B** Total homogenization temperature versus calculated mol% CO_2/CO_2+CH_4 content of type 1 inclusions

Oxygen and carbon isotope analyses

The $\delta^{18}O$ values of ten scheelite-bearing quartz samples are presented in Table 3, together with the $\delta^{18}O$ composition of H_2O in equilibrium with quartz at 250 °C and 350 °C, and the $\delta^{13}C$ isotope values of CO_2 extracted from fluid inclusions. For the measurement of $\delta^{18}O$ values, oxygen was liberated by reaction with BrF_5, and O_2 converted to CO_2 before mass-spectrometric analysis (Clayton and Mayeda 1963). Mass-spectrometry was performed on a Varian MAT 250 Triple collector instrument at the Geological Institute, University of Copenhagen, Denmark. Replicate determinations were done on 50% of the presented analyses and the mean deviation was 0.2‰.

The $\delta^{18}O$ value (in SMOW per mil) of quartz from the two scheelite mineralizations examined show a narrow range from 11.7 to 12.6, with no significant difference between the two mineralizations.

The $\delta^{13}C$ value (in PDB) per mil of CO_2 extracted from fluid inclusions range from −0.7 to +0.5, except for two values at +3.4 and +4.3 from the Kalogrias-Livadi mineralization (Table 3).

Discussion of results

Three types of fluid inclusions have been observed in both type I quartz and scheelite in quartz-veins from the scheelite mineralizations in the Metaggitsi area: type 1 aqueous-carbonic inclusions, type 2 carbon dioxide inclusions, and type 3 aqueous inclusions. The three types of fluid inclusions coexist in the same setting in most samples. This suggests a general contemporaneity of the three primary or pseudosecondary types of fluids. Textural observations furthermore suggest that type I quartz and scheelite have coprecipitated and that the fluids represented by primary types 1 and 2 inclusions represent the fluids from which scheelite precipitated. The compositional continuum shown in Fig. 8A strongly suggests close genetic relationship and contemporaneity among these fluids.

Decrepitation pressures of 1.6 kbar for the 10 μm type 1 inclusions, and 1.2 kbar for 20 μm type 1 inclusions were calculated on the basis of experimental data on the relationship between inclusion size and the decrepitation pressure of fluid inclusions in natural quartz (Bodnar et al. 1989). Considering that fluid inclusions in this study homogenize very close to their decrepitation point (Fig. 6D), it is suggested that minimum homogenization pressures were between 1.2 and 1.6 kbar. The FLINCOR (Brown 1989) program was used to calculate the pressure at homogenization for type 1 inclusions. Using the Brown and Lamb (1989) equation of state, calculated pressures range from 1.1 to 3.5 kbar and cluster around a median value of 2.2 kbar.

Table 3 Isotopic composition of oxygen ($\delta^{18}O$ SMOW, per mil) of quartz and calculated coexisting H_2O at 250 °C and 350 °C, and of carbon($\delta^{13}C$ PDB, per mil) from fluid inclusions in quartz

Location	Sample	$\delta^{18}O$ of quartz	$\delta^{18}O$ SMOW (per mil)		$\delta^{13}C$ PDB (per mil)
			$\delta^{18}O$ of water (250 °C)[a]	$\delta^{18}O$ of water (350 °C)[a]	$\delta^{13}C$ of fluid inclusion
Salonikio	SALI 101	12.6	3.7	5.7	−0.7
Salonikio	SALG 102	12.1	3.2	5.1	−1.0
Salonikio	SALF 103	12.3	3.4	5.4	−1.0
Salonikio	SALH 104	–	–	–	0.5
Salonikio	SALE 106	11.7	2.8	4.8	−0.7
Salonikio	SALC 107	11.8	2.9	4.9	−0.9
Salonikio	SALA 108	12.3	3.4	5.4	−0.3
Kalog. Livadi	SAL 24	12.3	3.4	5.4	−0.4
Kalog. Livadi	SAL 28	11.7	2.8	4.8	−1.2
Kalog. Livadi	SAL 29	12.2	3.3	5.3	3.4
Kalog. Livadi	SAL 30	12.1	3.2	5.1	4.3
Vrachoto	SV 1	–	–	–	0.2

[a] Fractionation equation of Matsuhisa et al. (1979)

Coexisting type 1 inclusions with highly variable CO_2/H_2O- phase ratios which homogenize into the H_2O or CO_2 phase over the same temperature range (Fig. 6D) strongly suggests the existence of a fluid which has undergone CO_2-H_2O phase separation prior to or during entrapment as fluid inclusions (Ramboz et al. 1982). Further evidence that type 1 inclusions represent the products of immiscibility is provided by the partitioning of CH_4, and CO_2, into the gas-rich (CO_2-rich) type 1 inclusions, and the conformity of end-member compositions trapped in type 1 inclusions to chemical equilibrium fractionation, at the minimum measured temperatures of homogenization, and calculated homogenization pressures.

In the system H_2O-CO_2-CH_4(-NaCl) at the two-phase boundary, methane is strongly partitioned into the vapour (CO_2-rich) phase, under medium to high grade metamorphic conditions (Naden and Shepherd 1989). This trend is shown by type 1 inclusions with a relatively higher calculated bulk $CO_2/CO_2 + CH_4$ molar ratio in the aqueous inclusions that homogenize into the H_2O phase, and a relatively lower $CO_2/CO_2 + CH_4$ ratio in the gas-rich inclusions that homogenize into the CO_2 phase (Fig. 8B).

According to the principles of chemical equilibrium any chemical species should be distributed between two immiscible fluid phases L (aqueous type 1) and V (gas-rich type 1) according to:

$$K_D,\, i^{\,LV} = (Xi^V/Xi^L)_{P,T}$$

where K_D: distribution coefficient and X: composition of species i (Ramboz et al. 1982)

The distribution coefficients, K_D, for each chemical species, were calculated from calculated bulk molar compositions of pairs of selected type 1 inclusions with the lowest measured homogenization temperatures best representing inclusions that have trapped immiscible pure end-member compositions (or the smallest amount of additional phases) (Table 4). The K_Ds display the distribution trend: K_D(NaCl) < K_D(H_2O) < K_D(CO_2) < K_D(CH_4) (Table 5) which may qualitatively be used to show immiscible phases (Diamond 1990). The observed differences in calculated homogenization pressures for the two pairs of selected type 1 inclusions (Table 4, see also Fig. 9) may be due to errors in inclusion-phases volume visual estimation, and/or fluid pressure variability resulting from opening and sealing, and deformation and fracturing, of the veins, or a time delay between entrapment of aqueous and gas-rich type 1

Table 4 Calculated bulk molar compositions and properties of selected type 1 inclusions representing pure end-member fluids produced by immiscibility in the system H_2O-CO_2-CH_4-NaCl (see text for discussion)

	Pair 1		Pair 2	
H_2O	87.50[a]	40.00[b]	90.90[c]	69.90[d]
CO_2	10.90	54.90	6.90	27.10
NaCl	1.10	0.40	1.80	0.62
CH_4	0.50	4.70	0.40	2.50
Wt.% NaCl equivalent	3.94	2.80	5.76	2.80
Density (g/cc)	0.91	0.65	0.90	0.78
Molar volume (cc/mole)	32.45	62.21	34.82	46.86

[a] Aqueous inclusion, H_2O homogenization at Th: 220 °C, Ph: 2.4 kbar
[b] Gas-rich inclusion, CO_2 homogenization at Th: 245 °C, Ph: 1.3 kbar
[c] Aqueous inclusion, H_2O homogenization at Th: 230 °C, Ph: 2.6 kbar
[d] Gas-rich inclusion, CO_2 homogenization at Th: 253 °C, Ph: 2.0 kbar

Table 5 Chemical distribution coefficients (K_D), calculated from data in Table 4 showing the relative trend K_D(NaCl) < K_D (H_2O) < K_D(CO_2) < K_D(CH_4) (see text for discussion)

Inclusion pair	K_D(NaCl)	K_D(H_2O)	K_D(CO_2)	K_D(CH_4)
1	0.36	0.45	5.03	9.40
2	0.34	0.76	3.92	6.25

$K_D, i^{LV} = (Xi^V/Xi^L)_{P,T}$ where:
K_D: distribution coefficient and X: composition of species i

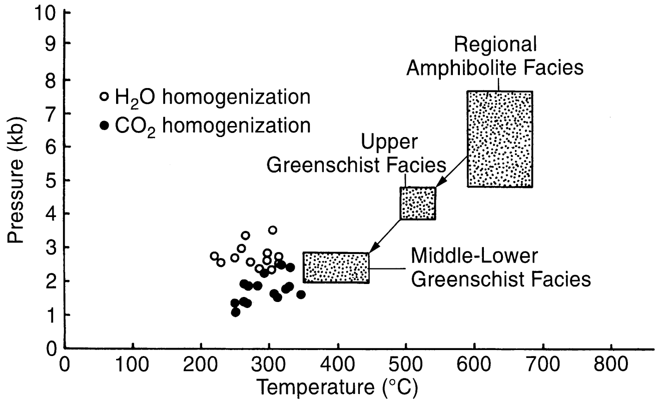

Fig. 9 Pressure-temperature diagram showing calculated homogenization conditions for type 1 inclusions in relation to inferred regional metamorphic conditions in the Metaggitsi region. Sources of data given in the text

inclusions, in a vein-system emplaced in a tectonically active environment (Robert and Kelly 1987; Diamond 1990).

Bulk fluid inclusion compositions were calculated in the system H_2O-CO_2-CH_4-NaCl (Table 4) on the basis of the method of Ramboz et al. (1985) using microthermometry data.

Since immiscibility has been strongly indicated, fluid inclusion homogenization and thus trapping conditions represent depositional conditions of quartz I and scheelite. Considering that for coeval inclusions, the minimum homogenization temperatures for inclusion homogenization into the H_2O, and into the CO_2, phases, are provided by inclusions trapping pure end-members (Table 4, Fig. 6D), these minimum homogenization T and P conditions of 220–250 °C at fluctuating pressures between 1.2 and 2.6 kbar can be safely considered as depositional conditions for scheelite. Some of the most aqueous-rich type 1 inclusions homogenizing at higher temperatures may represent trapping of homogeneous fluids. Calculated pressures at the homogenization temperature for these inclusions are higher than the rest of type 1 inclusions (see Fig. 9).

The mineralizing fluid densities and P-T conditions of vein formation are not compatible with regional amphibolite facies conditions (5–8 kbar; 600–800 °C), however, but more closely approach those of the retrogressive greenschist facies (2–3 kbar; 350–400 °C) conditions thus indicating that vein emplacement conceivably could be related to the late metamorphic/retrogressive greenschist facies conditions (Fig. 9).

$\delta^{18}O$ values of vein quartz

The $\delta^{18}O$ values of quartz and the calculated $\delta^{18}O$ values of coexisting waters at 250 °C and 350 °C (Table 3) do not constrain the origin of the waters uniquely. These values are depleted relative to purely magmatic waters (5.5 to 10 per mil, Taylor 1979) and overlap with the lowermost values of metamorphic fluids (3 to 20 per mil, Sheppard 1986). Moreover, oxygen isotope water compositions of less than or equal to 3.0 per mil are normally regarded as evidence for the presence of, or interaction with, isotopically light fluids such as meteoric waters (Landis and Rye 1974; Shepherd et al. 1976; Shelton et al. 1987). Calculated $\delta^{18}O_{water}$ values are interpreted to represent water from any source that has equilibrated isotopically with metasedimentary host rocks at low to moderate water-to-rock ratios.

$\delta^{13}C$ values of carbonic fluid

The $\delta^{13}C$ values of CO_2 fall in two groups, one from −1.5 to +1.5 per mil, the second with values of +3.4 and +4.3 per mil (Table 3). Excluding the latter two values the average $\delta^{13}C$ value is 0.15 ± 0.55 per mil. Various authors have suggested the following possible sources for CO_2 in hydrothermal fluids with such values:

1. Metamorphic decarbonation or dissolution reactions of carbonate (Ohmoto and Rye 1979). The $\delta^{13}CO_2$ value of such a metamorphic fluid will depend on the degree of decarbonation or dissolution, the $\delta^{13}C$ value of the carbonate minerals, and the isotopic fractionation factor between CO_2 and the carbonate mineral that is temperature dependent (Ohmoto 1986). According to Bottinga (1968) and Kerrich (1990) CO_2 liberated by such reactions at 400 °C to 500 °C would be enriched by about 3 per mil relative to the source. Carbon isotope values of Greek marbles range from −2 to +6 per mil with most values clustering between 0 and +4 per mil (Germann et al. 1980). The upper marble horizon of the Kerdilia Formation considered to have been subjected to similar tectonometamorphic processes with the Vertiskos Formation have $\delta^{13}C$ values between −3.5 and +4.1 per mil, with an average value of 0.9 per mil (Kalogeropoulos et al. 1989). Consequently, liberated CO_2 can be expected to have $\delta^{13}C$ values >0 per mil. In addition carbon isotope data for calcites of synvolcanic sea-floor alteration of basaltic origin, metamorphosed to low amphibolite or low- to mid-greenschist facies indicate $\delta^{13}C$ values ranging from −2.1 to +1.4 per mil (Groves et al. 1984). Considering that high-temperature dissolution in such low-carbonate rocks produces CO_2 that is isotopically similar to or slightly heavier than the original carbonate (Ohmoto and Rye 1979), sea-floor carbonate may produce CO_2 with $\delta^{13}CO_2$ close to 0 per mil. Ohmoto (1986) has calculated that under most geologic conditions the $\delta^{13}C$ value of CO_2 derived from carbonate rocks may fall between −8 and +4 per mil.
2. Oxidation of organic carbon in the rocks during metamorphism. According to Schidlowski (1988) the bulk of $\delta^{13}C$ values for organic carbon are −26 ± 7 per mil throughout the geologic record. Fluid buffered by graphite at 300 °C to 500 °C could have $\delta^{13}C$

values of -13 ± 2 per mil at equilibrium (Bottinga 1968; Ohmoto and Kerrick 1977). Also CO_2 $\delta^{13}C$ values of -1 to -5 per mil might be expected if CO_2 from a decarbonation source exchange with graphite or mixed with CO_2 resulting from oxidation of graphite. However, mass balance calculations indicate that rather large amounts of graphite are needed to produce $\delta^{13}C$ values between -1 and -5 per mil (Kreulen 1980);

3. CO_2 may be of deep-seated origin and represent either juvenile CO_2, possibly derived from degassing of the upper mantle (Touret 1981), or magmatic CO_2 (Ohmoto and Rye 1979; Taylor 1986). Juvenile CO_2 is generally accepted to have $\delta^{13}C$ values between -3 and -8 per mil based on isotopic analyses of carbonatites (Deines and Gold 1973), and diamonds (Deines 1980; Milledge et al. 1983). The characteristic $\delta^{13}C$ value of most magmatic-melt carbon is generally considered as being between -8 and -5 per mil (Taylor 1986). Kreulen (1980), in a study of the Naxos metamorphic terrain in Greece, identified a population of CO_2-rich fluids occurring in low- to high-grade schists, and pegmatites, with $\delta^{13}C$ values of -5 to -1 per mil, as probably of deep seated origin.

On the basis of these, $\delta^{13}C$ values of zero to greater are consistent with CO_2 of metamorphic origin produced during metamorphic decarbonation reactions. Concerning the slightly negative values down to -1.5 per mil (Table 3), if they are not due to decarbonation only, they most probably represent mixing of CO_2 produced by decarbonation with CO_2 from a deep seated source. Isotopic equilibration of graphite with carbon in CO_2 is not considered likely, due to the comparatively high measured $\delta^{13}C$ values, and the lack of graphite horizons within the rock assemblage hosting the tungsten mineralization.

Based on oxygen and carbon isotope evidence, a metamorphic model may account for the source of mineralizing fluids; this is in line with an in situ fluid evolution and origin from metamorphic reactions.

Model of scheelite concentration

On the basis of geochemical, textural, and field criteria, the lithologies of the Metaggitsi area, composed of intercalated metaclastic, and mafic and felsic metavolcanic rocks, have been recognized as representing metamorphic equivalents of submarine volcanosedimentary sequences (Veranis and Bitzios 1984). The occurrence of tourmaline-rich horizons, chemical metasediments (banded iron formations, chert) and stratabound scheelite disseminations, within the volcano-sedimentary units of the Metaggitsi area, may be interpreted as evidence for pre-metamorphic submarine exhalative processes (Slack 1982; Plimer 1983, 1987). This is supported by the lack of any evaporitic, pegmatitic, or granitic rocks within or close to the stratigraphic position of the tourmaline-rich rocks (Plimer 1983). Felsic dikes in the area of Metaggitsi, showing no relationship to igneous activity, may be products of fluid-rich metamorphic processes (Raith 1988). Submarine exhalative processes in volcano-sedimentary settings with accompanying boron (tourmaline) enrichment, are known to be genetically connected to pre-metamorphic syngenetic scheelite mineralization in various metamorphic terraines [e.g. in the Early Paleozoic Austroalpine Crystalline Complex, Eastern Alps (Raith 1988), the Lower-Middle Proterozoic Broken Hill Block, Australia (Plimer 1987), or the Archean Malene supracrustals, Greenland (Appel 1985)]. Furthermore, magmatic processes associated with island-arc boninites and tholeiites, are considered responsible for tungsten precipitation in the amphibolite-facies Early Paleozoic Habach Formation, Austria, hosting the Mittersill scheelite deposit (Thalhammer et al. 1989). It is thus reasonable to suggest an initial pre-metamorphic syngenetic scheelite mineralization also in the Metaggitsi lithologies.

Fluid inclusions similar to those of the Metaggitsi system are found in metamorphic rocks and vein (W and Au) deposits thought to be genetically related to regional metamorphic processes. Several studies summarized in Crawford (1981), Roedder (1984) and Crawford and Hollister (1986) indicate that CO_2- and/or H_2O-dominated fluids are characteristic of greenschist and amphibolite facies metasedimentary rocks. Metamorphic fluids have salinities that range between 2 and 6 or 20 and 25 equivalent weight % NaCl in pelitic schists and gneisses, and calcareous rocks, respectively. Higher salinities are often related to contamination from evaporitic rocks, or immiscibility. In addition, H_2O-CO_2 metamorphic fluids may be produced from rocks of basaltic composition at the greenschist-amphibolite facies transition at 500 °C (Kerrich and Fyfe 1981); such fluids will be characterized by low salinities due to the low Cl-contents of basaltic rocks. Fluid inclusion data from Mittersill (Schenk et al. 1990), indicate that the ore-forming fluids associated with amphibolite facies Alpine metamorphism of the host mafic metavolcanics, were CO_2-rich aqueous solutions with salinities between 2.2 and 7.8 equivalent weight % NaCl and containing also minor concentrations of CH_4. Lattanzi et al. (1989) , and Craw et al. (1993) report CO_2-rich inclusions of moderate salinity (5–11 equivalent weight % NaCl) characterized by immiscibility phenomena from gold-bearing veins of the eastern and northwestern Alps, Italy, associated with late-Alpine metamorphism of the host metasedimentary and metagranitic rocks. Immiscibility of CO_2-H_2O(-CH_4) fluids, containing 4–6 equivalent weight % NaCl, have also been reported from gold-bearing veins in metavolcanic-sedimentary sequences in the northwestern Italian Alps, and considered to be associated with late retrograde greenschist facies metamorphism and tectonic uplift (Diamond 1990). Furthermore, Paterson (1986) has described low-salinity CO_2-bearing inclusions in late Au-W(scheelite)-Sb vein deposits hosted by greenschist to amphibolite facies

Paleozoic metavolcanic-sedimentary schists, in New Zealand, that are considered to have been formed from fluids released during uplift of the metamorphic pile. Mobilization of scheelite from a pre-existing primary mineralization has been experimentally demonstrated during greenschist (and by inference amphibolite) facies *P-T* conditions (Foster 1977). Accordingly, the amphibolite-hosted scheelite ore-deposit of Mittersill, Austria, and stratabound scheelite mineralization in the polymetamorphic Austroalpine Crystalline Complex of the Eastern Alps have been ascribed to Alpine metamorphic remobilization of pre-concentrated scheelite (Raith 1988; Thalhammer et al. 1989). Therefore, combined with geologic evidence and O and C isotope data, the fluid inclusion data of the Metaggitsi scheelite vein-mineralization are consistent with vein genesis in the late stages of retrogressive greenschist facies metamorphism, by metamorphic fluids produced by devolatilization of deep portions of the Vertiskos crustal rocks. This is supported by the lack of any unequivocal evidence for deep seated magmatism in the area of Metaggitsi. However, if the Vertiskos Formation has indeed been affected by an earlier high *P-T* Hercynian metamorphism, and considering the possible Tertiary age of the mineralization, the source of fluids should be sought in dehydrating Circum-Rhodope Belt metasediments and metavolcanics, entrapped within an uplifted wedge pile such that probably represented by the Kerdilia Formation (Kalogeropoulos et al. 1989).

Oxygen fugacity calculations

Fugacities of oxygen for the entrapped fluids can be calculated from the bulk chemical compositions given in Table 1 in the system H_2O-CO_2-CH_4, along the *P*, *T* paths indicated for individual inclusions. The calculations were made for two inclusions considered to represent end-member immiscible compositions. The basic assumptions inherent in the calculations are analyzed in Konnerup-Madsen et al. (1985). The calculations of the possible $\log(fO_2)$ conditions for equilibration of the examined fluids were performed, assuming chemical equilibrium between the CO_2, H_2O and CH_4 in the inclusions via the reaction $CO_2 + 2H_2O = CH_4 + 2O_2$. Oxygen fugacities for type 1 fluid compositions of 10^{-35} to 10^{-31} bar are indicated for temperatures between 260 °C and 310 °C, that is values slightly above the synthetic Ni-NiO buffer curve.

Conclusions

The principal conclusions of this study are:

1. Scheelite mineralization accompanied by muscovite and albite, and traces of Mo-stolzite, stolzite, arsenopyrite, pyrite and iron oxides occurs in quartz vein systems of Alpine age, hosted by two-mica gneissic schists, and locally amphibolites, of the Paleozoic or older Vertiskos Formation in the Metaggitsi area, central Chalkidiki Peninsula, in N Greece.
2. Vein quartz shows evidence of slight to intense deformation manifested by undulose extinction, sutured quartz-quartz boundaries, translation gliding (type I), and in extreme cases incipient recrystallization (type II). Scheelite-quartz contacts, common slight to moderate undulose extinction, as well as similar fluid inclusion characteristics suggest that scheelite and type I quartz have coprecipitated. Small scale (2–3 cm wide) wallrock alteration haloes are characterized by intense potassium and hydrogen metasomatism manifested by replacement of plagioclase by sericite.
3. Scheelite was deposited from H_2O-CO_2 fluids undergoing phase separation at temperatures of 220 °C to 250 °C and pressures fluctuating between 1.2 and 2.6 kbar, and post-dating regional amphibolite facies metamorphism. The mineralizing fluids are characterized by high but variable contents of CO_2, small CH_4 content (generally <2 mol%), and aqueous phase salinity ranging between 0.2 and 8.3 equivalent weight% NaCl. Fluid oxygen fugacities during mineralization varied from 10^{-35} to 10^{-31} bar above the Ni-NiO buffer curve. The CO_2 fluid does not reflect equilibration with graphite.
4. Estimated $\delta^{18}O_{water}$ values of the hydrothermal fluid and $\delta^{13}C$ values of CO_2 in the inclusions of 3–6 per mil SMOW, and −1.2 to +4.3 per mil PDB, respectively, combined with fluid inclusion and geologic data, indicate that the mineralizing fluids have, at least partly, equilibrated with the metamorphic country rocks.

Acknowledgments This research was supported by a Danish Government Doctoral Scholarship to SK. Special acknowledgment goes to Dr. P. M. Holm of the Geological Institute, Copenhagen, for his patient help with the use of the fluorination line. Special thanks are extended to Dr. R. Kreulen of the University of Utrecht for his invaluable help with carbon isotope analyses of inclusion volatiles, and Dr. J. Dubessy of CREGU, Nancy, for the Raman Spectroscopy. The use of laboratory facilities at Copenhagen University was kindly supported by the Danish National Research Council. Special thanks are also extended to N. Veranis of the Institute of Geology and Mineral Exploration of Greece for his help in the field and for invaluable discussions on the local geology. We thank Dr. J. Naden, Dr. V. Gallagher, and Dr. R. Bodnar for constructive and detailed reviews of earlier drafts of this paper.

References

Angus S, Armstrong B, de Reuck KM (1976) International thermodynamic tables of fluid state 3: carbon dioxide. Pergamon, Oxford, 386 p

Appel PWU (1985) Strata-bound tourmaline in the Archean Malene supracrustals, West Greenland. Can J Earth Sci 22: 1485–1491

Bodnar RJ, Binns PR, Hall DL (1989) Synthetic fluid inclusions-VI. Quantitative evaluation of the decrepitation behaviour of

fluid inclusions in quartz at one atmosphere confining pressure. J Metam Geol 7: 229–242
Bottinga Y (1968) Calculation of fractionation factors for carbon and oxygen exchange in the system calcite-carbon dioxide-water. J Phys Chem 72: 4338–4340
Bottrell SH, Shepherd TJ, Yardley BWD, Dubessy J (1988) A fluid inclusion model for the genesis of the ores of the Dolgellau gold belt, North Wales. J Geol Soc 145: 139–145
Brauer R (1984) Preliminary report about the structural investigations in the Servo-Macedonian massif of the E Chalkidiki. Unpubl Rep IGME, Athens, 12 p
Brown PE (1989) FLINCOR: A microcomputer program for the reduction and investigatio n of fluid inclusion data. Am Mineral 74: 1390–1393
Brown PE, Lamb WM (1989) P-V-T properties of fluids in the system H_2O-CO_2-NaCl: new graphical presentations and implications for fluid inclusion studies. Geochim Cosmochim Acta 53: 1209–1221
Burruss RC (1981) Analysis of phase equilibria in C-O-H-S fluid inclusions. In: Hollister, LS, Crawford, ML (eds) Short course in fluid inclusions: applications to petrology. Mineral Assoc Canada 6: 39–74
Christofides G, d'Amico C, del Moro A, Eleftheriadis G, Kyriakopoulos C (1990) Rb/Sr geochronology and geochemical characters of the Sithonia plutonic complex (Greece). Eur J Mineral 2: 79–87
Collins PLF (1979) Gas hydrates in CO2-bearing fluid inclusions and the use of freezing data for estimation of salinity. Econ Geol 74: 1435–1444
Clayton RN, Mayeda TK (1963) The use of bromine pentafluoride in the extraction of oxygen from oxides and silicates for isotopic analysis. Geochim Cosmochim Acta 27: 43–52
Craw D, Teagle DAH, Belocky R (1993) Fluid immiscibility in late-Alpine gold-bearing veins, eastern and northwestern European Alps. Mineral Deposita 28: 28–36
Crawford ML (1981) Phase equilibria in aqueous fluid inclusions. In: Hollister LS, Crawford ML (eds) Short course in fluid inclusions: applications to petrology. Mineral Assoc Can 6: 75–100
Crawford ML, Hollister LS (1986) Metamorphic fluids: the evidence from fluid inclusions. In: Walther JV, Wood BJ, (eds) Fluid-rock interactions during metamorphism, Advances in physical geochemistry. Springer-Verlag, Berlin Heidelberg New York 5: 1–35
Deer WA, Howie RA, Zussman G (1966) An introduction to the rock forming minerals. Longman, 528 p
Deines P (1980) The carbon isotopic composition of diamonds, relationship to diamond shape, color, occurrence and vapor composition. Geochim Cosmochim Acta 44: 943–961
Deines P, Gold DP (1973) The carbon isotopic composition of carbonatite and kimberlite carbonates and their bearing on the composition of deep seated carbon. Geochim Cosmochim Acta Oxford 37: 1707–1733
Delhaye M, Dhamelincourt P (1975) Raman microprobe and microscope laser excitation. J Raman Spectrosc 3: 33–43
Diamond LW (1990) Fluid inclusion evidence for P-V-T-X evolution of hydrothermal solutions in late-Alpine gold-quartz veins at Brusson, Val D'Ayas, NW Italian Alps. Am J Sci 290: 912–958
Dimitriadis S, Godelitsas A (1991) Evidence for high pressure metamorphism in the Vertiscos group of the Serbomacedonian massif: the eclogite of Nea Roda. Bull Geol Soc Greece XXV/2: 67–80
Dixon JE, Dimitriadis S (1984) Metamorphosed ophiolitic rocks from the Servo-Macedonian Massif, near Lake Volvi, NE Greece. In: Dixon JE, Robertson AHF (eds) The geological evolution of the eastern Mediterranean, Special Publication of the Geological Society 17. Blackwell, pp 603–618
Foster RP (1977) Solubility of scheelite in hydrothermal chloride solutions. Chem Geol 20: 27–43
Fournaraki A (1981) Mineralogical and petrological study of amphibolitic rocks of the Servomacedonian Massif. Unpubl Ph D Thesis, University of Thessaloniki, Greece, 231 p
Frei R (1986) Geological, mineralogical and geochemical investigations of a strata-bound polymetallic mineralization and banded iron formation in the Servo-Macedonian Massif (Metaggitsi-Plana-Pyrgadikia, Chalkidiki). Unpubl Diploma thesis, University of Zurich, 102 p
Frei R (1992) Isotope geochemical investigations on Tertiary intrusives and related mineralizations in the Servomacedonian Pb-Zn, Sb + Cu-Mo metallogenetic province in Northern Greece. Unpubl Ph D Thesis, ETH Zurich, 220 p
Germann K, Holtzmann G, Winkler J (1980) Determination of marble provenance: limits of isotopic analysis. Archeometry 22: 99–106
Groves DI, Phillips GN, Ho SE, Henderson CA, Clark ME, Woad GM (1984) Controls on distribution of Archean hydrothermal gold deposits in Western Australia. In: Foster RP (ed) Gold'82: the geology, geochemistry, and genesis of gold deposits. Balkema, Rotterdam, pp 689–712
Hedenquist JW, Henley RW (1985) The importance of CO_2 freezing point measurements of fluid inclusions: evidence from geothermal systems and implications for epithermal ore deposition. Econ Geol 80: 1379–1406
Herzberg G (1951) Molecular spectra and molecular structure. II. Infrared and Raman Spectra. Van Nostrand Reinhold Company
Kalogeropoulos SI, Kilias SP, Bitzios D, Nicolaou M, Both RA (1989) Genesis of the Olympias carbonate-hosted Pb-Zn(Au, Ag) sulfide ore deposit, E Chalkidiki peninsula, N. Greece. Econ Geol 84: 1210–1234
Kaufmann G, Kockel F, Mollat H (1976) Notes on the stratigraphic and paleographic position of the Svoula Formation in the innermost zone of the Hellenides (N. Greece). Bull Soc Geol France (VII) 18: 225–230
Kerrich R (1990) Carbon-isotope systematics of Archean Au-Ag vein deposits in the Superior Province. Can J Earth Sci 27: 40–56
Kerrich R, Fyfe WS (1981) The gold-carbonate association: the source of CO_2 and CO_2 fixation reactions in Archean lode deposits. Chem Geol 33: 265–294
Kilias SP (1991) Metallogeny of polymetallic sulfide and tungsten mineralizations in the Servo-Macedonian Massif, N Greece: The examples of the Olympias Pb-Zn (Au, Ag) sulfide and the Metaggitsi scheelite deposits. Unpubl PhD Thesis, University of Copenhagen, 220 p
Kockel F, Molat H, Walther H (1977) Erlanterungen zur geologiscen Karte der Chalkidiki und angrenzender Gebiete 1:100000, Nordgriechenland. Bundesamt Geowiss Rohst Hannover, 119 p
Konnerup-Madsen J, Dubessy J, Rose-Hansen J (1985) Combined Raman microprobe spectrometry and microthermometry of fluid inclusions in minerals from igneous rocks of the Gardar province (south Greenland). Lithos 18: 271–280
Kougoulis H (1986) Retrograde metamorphism and determination of protoliths of Vertiscos Formation, Servomacedonian Massif (North of Volvi Lake and Lipsidrio-Laodikino). Unpubl Rep IGME, Athens, Greece, 73 p (in Greek)
Kougoulis H, Dabitzias S, Papadopoulos C (1989) (1) Geologic and metallogenetic study of amphibolites of the Servo-Macedonian Massif which are not related to ophiolitic complexes; (2) Geologic study (source) of isolated serpentinite bodies of the Servo-Macedonian Massif, and their metallogenetic significance. Unpubl Rep IGME, Athens, Greece. 108 p (in Greek)
Kreulen R (1980) CO_2-rich fluids during regional metamorphism on Naxos, a study on fluid inclusions and stable isotopes. Unpubl Ph D thesis. University of Utrecht, 85 p
Landis GP, Rye RO (1974) Geologic, fluid inclusion and stable isotope studies of the Pasto Bueno tungsten-base metal ore deposit, northern Peru. Econ Geol 69: 1025–1059
Lattanzi PF, Curti E, Bastogi M (1989) Fluid inclusion studies on the gold deposits of the Upper Anzasca Valley, northwestern Alps, Italy. Econ Geol 84: 1382–1397
Matsuhisa Y, Goldsmith JR, Clayton RN (1979) Oxygen isotopic fractionation in the system quartz-albite-anorthite-water. Geochim Cosmochim Acta 43: 1131–1140

Milledge HJ, Mendelssohn MJ, Seal M, Rouse JE, Swart DK, Pillinger CT (1983) Carbon isotope variation in spectral type II diamonds. Nature 303: 791–792
Naden J, Shepherd T (1989) Role of methane and carbon dioxide in gold deposition. Nature 342: 793–795
Ohmoto H, Kerrick D (1977) Devolatilization equilibria in graphitic systems. Am J Sci 277: 1013–1044
Ohmoto H, Rye RO (1979) Isotopes of sulfur and carbon. In: Barnes HL (ed) Geochemistry of hydrothermal ore deposits, 2nd edn. Springer, Berlin Heidelberg New York, pp 509–567
Ohmoto H (1986) Stable isotope geochemistry of ore deposits. In: Valley JW, Taylor HPJr, O'Neil JR(eds) Stable isotopes in high temperature geological processes. Mineral Soc Am 16: 491–561
Papadopoulos C (1982) Geologie des Servo-Mazadonischen Massivs, nordlich des Volvi-See, N. Griechenland. Unpubl Ph D Thesis, University of Vienna, 176 p
Papadopoulos C, Kilias A (1985) Altersbeziehungen zwischen Metamorphose und deformation im zentralen teil des Serbomazedoniscen Massivs (Vertiscos-Gebirge, Nord-Griechenland). Geol Rundsch 74: 77–85
Paterson CJ (1986) Controls on gold and tungsten mineralization in metamorphic-hydrothermal systems, Otago, New Zealand. In: Duncan Keppie J, Boyle RW, Haynes SJ (eds) Turbidite-hosted gold deposits: GAC Spec Pap 32: 25–40
Patras D, Kilias A, Chadzidimitriadis E, Mundrakis D (1986) Study of the formation phases of the internal Hellenides in Northern Greece. Bull Geol Soc Greece XX: 139–157 (in Greek with English abstr)
Plimer IR (1983) The association of tourmaline-bearing rocks with mineralization at Broken Hill, N.S.W. Proc Aust Inst Min Metall Conf, Broken Hill, pp 157–176
Plimer IR (1987) The association of tourmalinite with stratiform scheelite deposits. Mineral Deposita 22: 282–291
Potter RW II, Clyne MA, Brown DL (1978) Freezing point depression of aqueous sodium chloride solutions. Econ Geol 73: 284–285
Poty B, Leroy J, Jachimowicz L (1976) Un nouveil appareil pour la mesure des temperatures sous le microscope: I: installation de microthermometrie Chaixmeca. Bull Mineral 99: 182–186
Raith JG (1988) Tourmaline rocks associated with stratabound scheelite mineralization in the Austroalpine Crystalline Complex, Austria. Mineral Petrol 39: 265–288
Ramboz C, Pichavant M, Weisbrod A (1982) Fluid immiscibility in natural processes: use and misuse of fluid inclusion data in terms of immiscibility. Chem Geol 37: 29–48.
Ramboz C, Schnapper D, Dubessy J (1985) The P-V-T-X-FO_2 evolution of H_2O-CO_2-CH_4 bearing fluid in a wolframite vein: reconstruction from fluid inclusion studies. Geochim Cosmochim Acta 49: 205–219
Robert F, Kelly WC (1987) Ore-forming fluids in Archean gold-bearing quartz veins at the Sigma mine, Abitibi greenstone belt, Quebec, Canada. Econ Geol 82: 1464–1482
Roedder E (1984) Fluid inclusions. Rev Mineral 12, 644 p
Sakellariou, D. (1988) Geologie des Serbomazedonischen Massivs in der nordostlichen Chalkidiki, N. Griechenland-Deformation und Metamorphose. Unpub Ph D Thesis, University of Mainz, 177 p
Schenk P, Holl R, Ivanova GF, Naumov VB, Kopneva IA (1990) Fluid inclusion studies of the Felbertal scheelite deposit. Geol Rundsch 79/2: 451–466
Shelton KL, Taylor RP, So CS (1987) Stable isotope studies of the Dae Hwa tungsten-molybdenum mine, Republic of Korea: evidence of progressive meteoric water interaction in a tungsten-bearing hydrothermal system. Econ Geol 82: 471–481
Schidlowski M (1988) A 3,800-million-year isotopic record of life from carbon in sedimentary rocks. Nature 333: 313–318
Schuneman M (1986) Contribution to the geology, geochemistry, and tectonics of the Chortiatis series metamorphic calc-alkaline suite, Chalkidiki, N. Greece. Unpubl Ph D Thesis, University of Hamburg, 182 p
Shepherd TJ, Beckinsale RD, Rundle CC, Durham J (1976) Genesis of the Carrock Fell tungsten deposits, Cumbria: fluid inclusion and isotopic study. Inst Min Metall Trans 85: 1363–1373
Sheppard SMF (1986) Characterization and isotopic variations in natural waters. In: Valley JW, Taylor HP Jr, O'Neil JR (eds) Stable isotopes in high temperature geological processes. Reviews in Mineralogy, Mineral Soc Am 16: 165–181
Slack JF (1982) Tourmaline in Appalachian-Caledonian massive sulfide deposits and its exploration significance. Trans Inst Min Metall 91: B81–B89
Taylor HP Jr (1979) Oxygen and hydrogen isotope relationships in hydrothermal mineral deposits. In: Barnes HL (ed) Geochemistry of hydrothermal ore deposits, 2nd edn. Wiley-Intersci, New York, pp 236–277
Taylor BE (1986) Magmatic volatiles: isotopic variation of C, H, and S. In: Valley JW, Taylor HP Jr, O'Neil JR (eds) Stable isotopes in high temperature geological processes. Mineral Assoc Am 16: 185–225
Thalhammer OAR, Stumpfl EF, Jahoda R (1989) The Mittersill scheelite deposit. Econ Geol 84: 1153–1171
Touret J (1981) Fluid inclusions in high grade metamorphic rocks. In: Hollister LS, Crawford ML (eds) Mineral Assoc Can 6: 182–208
van den Kerkhof F (1990) Isochoric phase diagrams in the systems CO_2-CH_4 and CO_2-N_2: applications to fluid inclusions. Geochim Cosmochim Acta 54: 621–629
Veranis N, Bitzios D (1984) Preliminary report on the geology and metallogenesis of the Pirgadikia-Metaggitsi-Salonikio area. Unpubl Rep IGME, Athens, 71 pp (in Greek)
Vital C (1986) Mineralogical and petrographical investigations of the area between Arnea and Megali Panagia, Chalkidiki Peninsula (N Greece). Unpubl Dipl Thesis, ETH Zurich, 125 pp